León *et al. Microbial Cell Factories* (2024) 23:248
https://doi.org/10.1186/s12934-024-02519-6

Microbial Cell Factories

RESEARCH Open Access

Microbial green synthesis of luminescent terbium sulfide nanoparticles using *E. Coli*: a rare earth element detoxification mechanism

Juan José León[1,2,3], Nía Oetiker[1,2,3], Nicolás Torres[1], Nicolás Bruna[1], Evgenii Oskolkov[1], Pedro Lei[3], Andrey N. Kuzmin[2], Kaiwen Chen[3], Stelios Andreadis[3], Blaine A. Pfeifer[3], Mark T. Swihart[3], Paras N. Prasad[2*] and José Pérez-Donoso[1*]

Abstract

Background Rare-earth sulfide nanoparticles (NPs) could harness the optical and magnetic features of rare-earth ions for applications in nanotechnology. However, reports of their synthesis are scarce and typically require high temperatures and long synthesis times.

Results Here we present a biosynthesis of terbium sulfide (TbS) NPs using microorganisms, identifying conditions that allow *Escherichia coli* to extracellularly produce TbS NPs in aqueous media at 37 °C by controlling cellular sulfur metabolism to produce a high concentration of sulfide ions. Electron microscopy revealed ultrasmall spherical NPs with a mean diameter of 4.1 ± 1.3 nm. Electron diffraction indicated a high degree of crystallinity, while elemental mapping confirmed colocalization of terbium and sulfur. The NPs exhibit characteristic absorbance and luminescence of terbium, with downshifting quantum yield (QY) reaching 28.3% and an emission lifetime of ~ 2 ms.

Conclusions This high QY and long emission lifetime is unusual in a neat rare-earth compound; it is typically associated with rare-earth ions doped into another crystalline lattice to avoid non-radiative cross relaxation. This suggests a reduced role of nonradiative processes in these terbium-based NPs. This is, to our knowledge, the first report revealing the advantage of biosynthesis over chemical synthesis for Rare Earth Element (REE) based NPs, opening routes to new REE-based nanocrystals.

Keywords Bacteria, Nanoparticles, Lanthanides, Rare earth elements, Terbium, Biosynthesis, Green synthesis

*Correspondence:
Paras N. Prasad
pnprasad@buffalo.edu
José Pérez-Donoso
jperezd@gmail.com
[1]BioNanotechnology and Microbiology Laboratory, Center for Bioinformatics and Integrative Biology (CBIB), Facultad de Ciencias de la Vida, Universidad Andres Bello, Santiago, Chile
[2]Department of Chemistry and the Institute for Lasers, Photonics, and Biophotonics, University at Buffalo, State University of New York, Buffalo, NY, USA
[3]Department of Chemical and Biological Engineering, University at Buffalo, State University of New York, Buffalo, NY, USA

Introduction

Lanthanide (Ln^{3+})-based NPs are employed in numerous technologies including radar, computer screens, drug-delivery systems, and high penetration bioimaging [1–3]. Many of these applications are based on their photoluminescence. Lanthanides with the most efficient downshifting visible luminescence include trivalent terbium, europium (Eu), and samarium (Sm) ions [4]. Their temporal and spectral properties (long lifetime, sharp emission bands, and large Stokes shifts) make them particularly useful in time-resolved luminescence bioassays. Their emission is easily distinguished from autofluorescence based on its much longer lifetime [5]. Although Tb is one of the most luminescent lanthanides, reports of synthesis of Tb-based NPs are rare.

NPs are commonly made through chemical synthesis, but the large solvent volumes and high temperatures needed for this approach often limit large scale application. Thus, green and more sustainable processes to synthesize Tb-containing NPs using biological systems at low temperature without toxic reagents or solvents are needed. A few methods to produce Tb-containing NPs have been reported, mostly based on chemical synthesis [6–8].

Metal sulfide NPs (MeS NPs) are used in applications such as antibacterial agents, imaging and diagnostics, photo- and chemotherapy, pharmacology, and the manufacture of biosensors [9]. Many Me-S NPs are biocompatible and exhibit physicochemical properties that are useful for biological applications [10]. Chitosan-capped TbS (CS-Tb_2S_3) NPs produced using a bottom-up chemical method were recently reported [6]. Chemical synthesis of REE-doped NPs of metal sulfides including CdS, ZnS, and PbS has been reported in several studies [11–15]. These REE-doped NPs form a new class of luminescent materials with narrow emission lines, a large separation between the excitation and emission wavelengths, and a long emission lifetime [16]. Thus, sulfide lattices have potential to be good hosts for Tb.

Studies of the interaction of REEs with cells or biomolecules have, to date, been limited. Some specific enzymes that interact and bind Ln^{3+} ions have been described. In this context, the identification, molecular structure, and nucleotide sequence of a Ce^{3+}-induced methanol dehydrogenase (MDH) from *Bradyrhizobium* sp [17] and the induction of MDH activity by La^{3+} ions on proteins exhibiting MDH activity in *Methylobacterium radiotolerans* [18] were reported. Later, the MDH gene homologue, *xoxF1*, was shown to be upregulated in response to La^{3+} exposure in *Methylobacterium extorquens* [19]. A highly selective Ln^{3+}-binding protein called lanmodulin (LanM) was identified in *M. extorquens* [20]. Despite these prior reports, the biological relevance of lanthanides remains unknown, and studies of their interactions with cells are needed.

Tb compounds are considered to be of low to moderate toxicity, but only a few reports about Tb interaction with biological systems have been published [21–23]. The minimal inhibitory concentrations of different Tb compounds against pathogenic bacteria have been described, with *Pseudomonas aeruginosa*, *Escherichia coli*, and *Staphylococcus aureus* showing MICs over 1 mM [24]. Tb biosorption and selectivity by a genetically modified *E. coli* strain expressing lanthanide binding tags on the cell surface has been reported [25, 26]. Just one study reporting the biological synthesis of Tb_2O_3 NPs, by incubating Tb_4O_7 with *Fusarium oxysporum* biomass has been published. *F. oxysporum* produces compounds with a very high reduction potential, which can reduce Tb_4O_7 in aqueous media, yielding Tb_2O_3 NPs with a 10 nm size [27].

To better characterize Tb-bacteria interactions, here we studied the effect of terbium on the growth and viability of *E. coli*. Based on this, we developed a green, simple, and non-toxic approach for the biosynthesis of small (<10 nm), downshifting luminescent terbium sulfide (TbS) NPs. By developing a biosynthesis method for TbS, this study provides (i) a methodology shift to more sustainable REE-nanoparticle production in contrast to current chemical approaches and ii) greater insight into REE-bacteria interactions.

Materials and methods

L-cysteine ≥ 98%, tryptone grade 200, yeast extract, glucose ≥ 99.5%, casaminoacids OmniPur® Grade, sodium chloride ≥ 99.0%, sodium pyruvate ≥ 99%, potassium sulfate ≥ 99.0% and magnesium sulfide ≥ 99.0% for cell culture media as well as terbium nitrate pentahydrate 99.9% trace metals basis were obtained from Sigma-Aldrich. Terbium nitrate stock solutions were filtered through 0.22-µm filters, and bacterial cell culture reagents were autoclaved prior to use.

Bacterial growth curves

E. coli BL21(DE3) cells were grown in LB or R2A media supplemented with different concentrations of terbium nitrate ($Tb(NO_3)_3$) at 37 °C with constant shaking (180 RPM). Bacterial growth was determined by measuring OD_{600nm} using a multimode microplate reader Synergy H1 (Biotek). The same bacterial strain was used for all experiments.

Cellular viability assays

E. coli was grown in LB or R2A media at 37 °C with constant agitation until OD_{600nm} = 0.6 was reached. At this point, cellular viability was evaluated in cells exposed to different concentrations of terbium nitrate and in

cultures exposed to conditions for NP biosynthesis (cysteine and terbium nitrate supplementation). In the first case, the culture was divided into several tubes with the desired concentration of terbium nitrate (1, 3, 5 or 10 mM). Then, an aliquot was taken to measure the colony forming units (CFUs) after 0 and 24 h of exposure. In the second case, when the culture reached an OD_{600nm} = 0.6, the bacterial cells were washed with deionized water and resuspended in one volume of borax-citrate buffer (disodium tetraborate 15 mM and trisodium citrate 15 mM, pH 9.4). The suspension was then supplemented with 1 mM cysteine and left at room temperature for 1 h without shaking. After this time, the culture was challenged with terbium nitrate 1, 3, or 10 mM and incubated at 37° C with continuous shaking. Aliquots were taken at 0 and 24 h to determine CFUs.

Sulfide detection in culture headspaces

Sulfide production by bacterial cells was determined following a previously described protocol [28]. Briefly, a sterile paper soaked in lead acetate (100 mM) was attached under the cap of tubes used for bacterial growth. Bacterial cultures were grown to OD_{600nm} = 0.6 in LB medium supplemented with cysteine (1 mM) and different concentrations of terbium nitrate (1, 3, and 10 mM) and then incubated for 30, 60, and 120 min at 37 °C. Sulfide (S^{2-}) production was visualized by the change in the color of the papers obtained for each condition and quantified using the Fiji-ImageJ software (http://imagej.nih.gov/ij/) based upon a grayscale calibration as described previously [29].

Auto-metallography assay

The biosynthesis of metal sulfide nanomaterials was evaluated by using an auto-metallography assay previously reported to detect lithium, gold, and zinc sulfide nanomaterials [29–31]. A Silver Enhancer kit (Sigma-Aldrich, SE-100) was used in the experiments. Purified TbS nanoparticles were exposed to the silver enhancer mixed solution for 10 min and centrifuged to remove the silver enhancing solution. Then, a sodium thiosulfate solution was added for 3 min, and the sample was observed using a microscope.

Biosynthesis of TbS NPs

E. coli was grown with agitation at 37 °C in fresh liquid LB media until the exponential phase was reached. This was determined through optical density measured at 600 nm (OD_{600nm} ~ 0.6). The cells were centrifuged, and the supernatant was discarded. The cell pellet was washed and resuspended in one volume of borax-citrate buffer (di-sodium tetraborate 15 mM and trisodium citrate 15 mM, pH 9.4) to obtain an OD_{600nm} = 0.6. The suspension was supplemented with L-cysteine 1 mM and held at room temperature for one hour to favor the production of hydrogen sulfide. Afterwards, 10 mM $Tb(NO_3)_3{\cdot}5\ H_2O$ was added to the solution, and the culture was incubated with agitation at 37 °C for one hour. During this time, the solution changed from transparent to a pale greenish color, indicating the formation of nanoparticles. Tb nitrate was first dissolved in water to generate a concentrated stock and then the appropriate volume was added to reach the mentioned final concentration.

To purify the NPs, the culture was centrifuged at 7.000 RPM twice, and the cell pellet was discarded. The supernatant was then filtered using a 0.22 µm filter. The NPs (from the solution passing through the filter) were washed with distilled water and concentrated using a 0.3 kDa MilliporeSigma™ Amicon™ Filter tube. Finally, the NPs were purified using a thiol Sepharose 4B affinity column. The logic behind the use of a thiol-sepharose 4B affinity column to purify the NPs was that if terbium sulfide NPs are being formed, then the sulfur groups present in the NPs should bind to the column. This solution with purified NPs was used for further characterization.

Characterization of biosynthesized TbS NPs

The emission spectra of purified NPs were measured under 350 nm excitation and recorded in the range of 390–800 nm, using a Synergy™ H1 multi-plate reader (BioTek Instrument Inc.). HR-TEM images of the NPs were obtained utilizing a JEOL JEM 2010 microscope and a Thermo Scientific Talos 200X microscope. This equipment provided bright and dark field morphology images and the corresponding SAED patterns. The samples were dispersed through bath sonication (15 min) and then deposited onto a carbon coated copper grid before microscope observation. The shape, size, and interplanar distance of the NPs were determined by processing HR-TEM micrographs with the software Fiji [32]. SAED ring patterns were further analyzed using the EDP2XRD software to convert them to equivalent X-ray diffraction (XRD) patterns [33]. The elemental mapping of the NPs was carried out with a Thermo Scientific Talos 200X electronic microscope equipped with four in-column SDD Super-X detectors for Energy Dispersive X-ray Spectroscopy (EDS) signal detection and chemical characterization with compositional mapping.

Fluorescence lifetime measurements

An MT5365-UV LED (Mouser Electronics, Inc., Mansfield, TX) 3.6mW@370nm connected to a LEDD1B power supply (ThorLabs, Inc.,Newton, NJ) was used to excite the TbS powder. Pulsed operation of the LED was triggered by a PM5712 pulse generator (Philips, Amsterdam, Netherlands). Emission relaxation was detected by an H6780-20 PMT from Hamamatsu Photonics (Japan) connected to a TDS5104B oscilloscope from Tektronix,

Inc. (Beaverton, OR). To distinguish excitation light and other background from green TbS emission, a bandpass optical filter, D560/40 from Chroma Technology Corporation (Bellows Falls, VT), was attached at the input window of the PMT.

Downshifting QY measurements

Absolute quantum yield values were obtained with a Horiba Fluorolog-QM spectrofluorometer equipped with a QuantaPhi-2 integrating sphere attachment. Spectralon® powder holder cups with quartz covers were used for the samples. An excitation wavelength of 379 nm was chosen based on the excitation spectra of TbS NPs powder. For emission peaks integration, the area of a given spectrum between 470 and 640 nm was chosen to include the characteristic Tb emission lines at 490, 546, 586, and 622 nm, thus, allowing calculation of the total downshifting quantum yield.

MTT cell viability assay

Human dermal fibroblasts isolated as described previously were seeded at 8,000 cells/well in 96-well tissue culture treated plates [34]. On the next day, cells were exposed to the indicated concentrations of TbS NPs or $Tb(NO_3)_3$. After 24 h, cells were replenished with fresh medium containing 10 mg/mL 3-(4,5-dimethylthiazol-2-yl)-2,5,-diphenyltetrazolium bromide (MTT). After 4–5 h, the medium was removed, and the cells were incubated in 10% (w/v) SDS at 37 °C overnight. Optical density ($OD_{570\text{-}650\ nm}$) was determined by using a Synergy 4 hybrid multi-mode microplate reader (Agilent, Santa Clara, CA). In separate assays (again after 24 h of cell culture).

Live/dead cell assay

Human dermal fibroblasts isolated as described previously were seeded at 8,000 cell/well in 96-well tissue culture treated plates [34]. On the next day, cells were exposed to the indicated concentrations of TbS or $Tb(NO_3)_3$. After 24 h, live/dead cells were determined using the LIVE/DEAD™ Viability/Cytotoxicity kit (Thermo Fisher Scientific) as per the manufacturer's protocol. Images of stained cells (live cells=green, calcein AM; dead cells=red, ethidium homodimer-1) and phase images were acquired using an Observer Z1 microscope (Carl Zeiss Inc, Thornwood, NY) equipped with a high-definition digital camera (ORCA-ER C4742-80, Hamamastu, Bridgewater, NJ).

Results

Analysis of Tb^{3+} effect upon *E. Coli* growth

We tested the effect of terbium nitrate on the growth of *E. coli* cells to determine a suitable range of metal concentrations for biosynthesis of Tb-containing NPs. This was evaluated in Luria Broth (LB) and Reasoner's 2 A agar (R2A) media. *E. coli* BL21(DE3) cultures were grown in the presence of increasing concentrations of terbium (0.005–10 mM) to assess the effect of the metal on bacterial growth curves. As shown in Supplementary Figure S1, increased concentrations of terbium affected the growth curves in both culture media, totally suppressing bacterial growth at concentrations of 4 mM in LB media and 1 mM in R2A media. Terbium nitrate growth MICs of 3.5 and 0.5 mM were determined for *E. coli* cells grown in LB and R2A media, respectively (Figure S1).

Analysis of Tb^{3+} effect upon *E. Coli* viability

Most methods to biosynthesize metal NPs expose bacterial cultures to the metal precursors during the exponential growth phase, a condition in which the culture contains a high concentration of bacterial cells (10^7 – 10^8 cells/mL) that are metabolically active before metal precursors are added. Thus, the effect of terbium nitrate on the viability of exponential cultures of *E. coli* cells grown in LB and R2A media was evaluated at the MIC values. This assay evaluated the toxicity of Tb upon bacteria that were grown to $OD_{600nm}=0.6$ prior to Tb addition. For cells grown in LB media, CFUs increased by an order of magnitude in 4 h in the control condition (no Tb added). The same increase was observed upon exposure to 1- and 3-mM terbium nitrate. However, cells exposed to 5 mM terbium nitrate retained only 5.8% cellular viability after 30 min. Total absence of viability was determined when the cells were exposed to 10 mM terbium nitrate (Figure S2A). In R2A media, a total loss of cell viability after 30 min was observed in cells exposed to 3-, 5-, and 10-mM terbium nitrate ($p<0.0001$). An 84.3% decrease in cell viability was observed after 4 h exposure to 1 mM terbium nitrate (Figure S2B). In general, cellular growth and viability of *E. coli* cells are less affected by Tb^{3+} in LB media than in R2A media.

Biosynthesis of TbS NPs

Effect of cysteine exposure prior to tb supplementation upon E. Coli viability

Our biosynthesis protocol takes advantage of the ability of some microorganisms to produce high concentrations of reactive sulfides from cysteine while suspended in borax citrate buffer [29, 35, 36]. Thus, to select the ideal conditions for TbS NP biosynthesis, we evaluated the effect of cysteine supplementation (1 mM) on the cellular viability of *E. coli* in the presence of different concentrations of terbium nitrate (1, 3, and 10 mM). After cysteine supplementation, the cellular viability of cells exposed to 1, 3, and 10 mM of Tb decreased by 1 to 2 orders of magnitude relative to the Tb-free control over a 1 h period (Supplementary Figure S3). Cysteine treatment enhanced the tolerance of cells to terbium at all concentrations

evaluated. This effect is most evident in cells exposed to 10 mM of Tb, a concentration that in the absence of cysteine produced a total loss of viability (Supplementary Figure S2A).

The effect of cysteine on sulfide production was confirmed by assaying the production of S^{2-} in the headspace of *E. coli* cultures. In this assay, lead present in the filter paper reacts with the sulfide in the headspace to darken the paper. All cultures exposed to cysteine presented a darker coloration compared to the control, confirming the generation of sulfide as previously reported [37]. Cultures exposed to terbium produced lower levels of sulfide than the Tb-free control, a result that is most evident after 30 min incubation (Figure S4). The exposure to 10 mM terbium clearly decreases the amount of sulfide present in the headspace of cultures (Figure S4B).

Evaluation of different concentrations of the REE NP precursor

We evaluated the emission of filtered, concentrated, and purified nanostructures (see methods) under 350 nm excitation using different concentrations of terbium nitrate. As shown in Supplementary Figure S5, the purified NPs exhibit the characteristic emission peaks of terbium. More details are given in the characterization section below.

Confirmation of metal sulfide nanostructures formation

Next, we confirmed the presence of sulfur in the NPs using an auto-metallography assay that detects the presence of chalcogenides in a sample by their reaction with silver (Supplementary Figure S6). Dark spots were observed in the samples with NPs, and the darkening increased in samples obtained from cells exposed to higher concentrations of terbium nitrate and cysteine. This result was also observed in positive controls containing CdTe and CdS nanoparticles but was not observed when only Tb was supplied (Supplementary Figure S7).

Characterization of biosynthesized TbS NPs

Spectroscopic characterization

A relevant feature of Tb^{3+} based nanomaterials is their interesting optical properties characterized by emission peaks associated with multiple $^5D \rightarrow ^7F$ transitions. Based on this, the emission spectra of purified TbS NPs produced by *E. coli* cells exposed to 10 mM terbium nitrate and 1 mM cysteine were evaluated. As shown in Fig. 1, the Tb characteristic emission peaks at 490 nm, 546 nm, 586 nm, and 622 nm under excitation at 350 nm were observed [38–40]. Measurements were performed and calculated for emission lines at 490 nm, 546 nm, 586 nm, and 622 nm. The total downshifting QY calculated was 28.3%.

A particular property of REE based nanomaterials is their long emission lifetime, a characteristic that is the basis for many of their applications. We evaluated the emission lifetime of the biosynthesized TbS NPs to be ~2 ms (Fig. 1C). We also evaluated the change in emission lifetime for NPs biosynthesized using different concentrations of the metal precursor. A slight increase in emission lifetime was observed for the NPs produced at lower Tb nitrate concentrations (Figure S8).

Morphology of the NPs

The size and shape of purified NPs produced by *E. coli* were determined by electron microscopy. TEM imaging showed that TbS NPs have a spherical shape with sizes below 10 nm (Fig. 2). A size histogram was constructed by analyzing 500 nanoparticles, yielding a mean size of 4.1 +/- 1.3 nm and a size distribution ranging from 2 to 10 nm (Fig. 2B).

Crystallinity of the NPs

HR-TEM and SAED were used to analyze the structure and crystallinity of the NPs. An interplanar distance of 0.3 nm was observed in the HR-TEM micrographs (Fig. 2D and E). In addition, a high-resolution micrograph was analyzed revealing that the sample is loaded with nanoparticles, and they are all crystalline (Figure S9). The obtained EDP patterns were transformed into an XRD pattern using a software for better analysis (Figure S10, Table S2, Figure S11 and Table S3).

Elemental analysis of the NPs

The elemental composition and distribution of the NPs was evaluated through EDS analysis. STEM-EDS elemental mapping of purified NPs confirmed that S and Tb are co-located in the TbS NPs (Fig. 2G and H). EDS quantification (Supplementary Table S4) showed a Tb to S ratio of 1.91, but this includes not only the NPs themselves, but the biomass in which they were embedded.

Cytotoxicity of TbS NPs

Finally, we evaluated the cytotoxicity of the NPs toward human fibroblasts as a representative human cell type. For comparison, cytotoxicity of the precursor, terbium nitrate, was also evaluated. Using the conventional MTT assay, we observed that when exposed to 0.625 mg/mL terbium nitrate, cell viability decreased by about 20% relative to control cells that were not exposed to the precursor. Increasing concentrations of Tb nitrate further reduced cell viability, resulting in almost no viable cells at concentrations ≥ 10 mg/mL. In contrast, exposure to TbS NPs revealed lower cytotoxicity than Tb nitrate (Supplementary Figure S12). At 0.625 mg/mL TbS NPs, cell viability was similar to cells not exposed to nanoparticles. At concentrations from 1.25 to 20 mg/mL TbS, cell viability

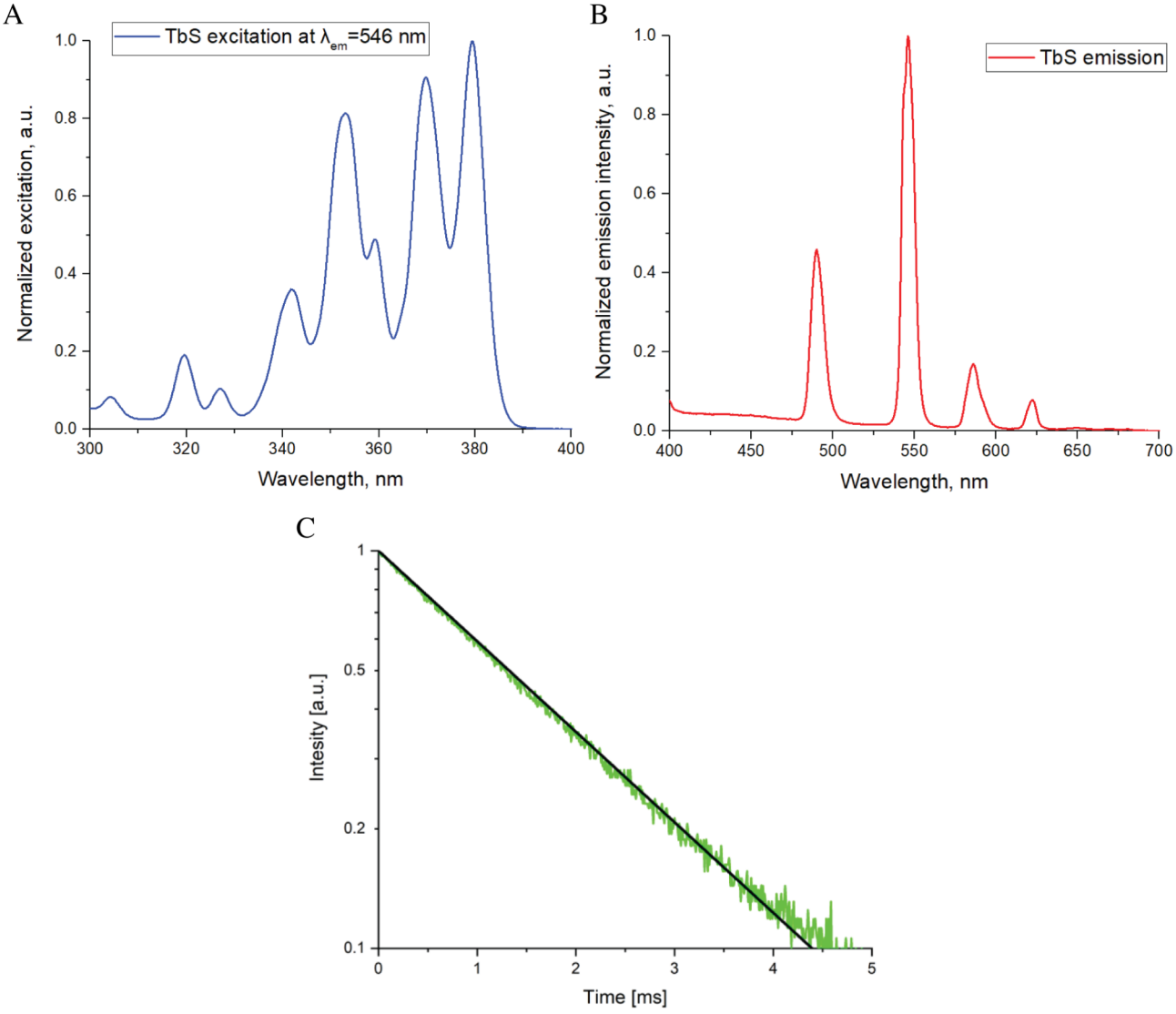

Fig. 1 Excitation and emission spectra, and emission lifetime measurement of freeze-dried purified TbS NPs produced by *E. coli*. (**A**) excitation spectrum measured at an emission wavelength of 546 nm, (**B**) emission spectrum measured at an excitation wavelength of 379 nm, and (**C**) emission decay measurement at an excitation wavelength of 350 nm. The black line shows a single-exponential fit with a lifetime of 1.91 ms

decreased by 30–40%. At the highest TbS concentration used (40 mg/mL), cell viability was less than 20% (Supplementary Figure S12).

A live/dead cell assay showed that after exposure to different concentrations of terbium nitrate (Supplementary Figure S13), Similar numbers of cells remained on the surface of the wells (phase contrast), while an increasing fraction of dead cells (stained red) was observed starting at a concentration of 5 mg/mL. In agreement with the MTT assay, at concentrations ≥ 10 mg/mL terbium nitrate, there were only dead cells but no live cells. In contrast, increasing concentrations of TbS NPs (Supplementary Figure S14) resulted in decreasing cell number (phase image), but most cells remained viable (green).

Discussion

Terbium was chosen among the lanthanides due to its excellent fluorescent and magnetic properties and because it is one of the most used and studied lanthanides in the manufacturing of NPs [41, 42]. Therefore, the aim of this study was to develop a green method for the biosynthesis of TbS nanoparticles using *E. coli* as a biofactory.

We assessed the tolerance of *E. coli* to terbium nitrate and determined a minimum inhibitory concentration (MIC) of 3.5 mM in LB media (Figure S1). This value indicates that Tb^{3+} is less toxic to *E. coli* cells compared to Cd^{2+}, Zn^{2+}, and Pb^{2+} (MICs of 1, 2, and 1.25 mM, respectively) [43–46].

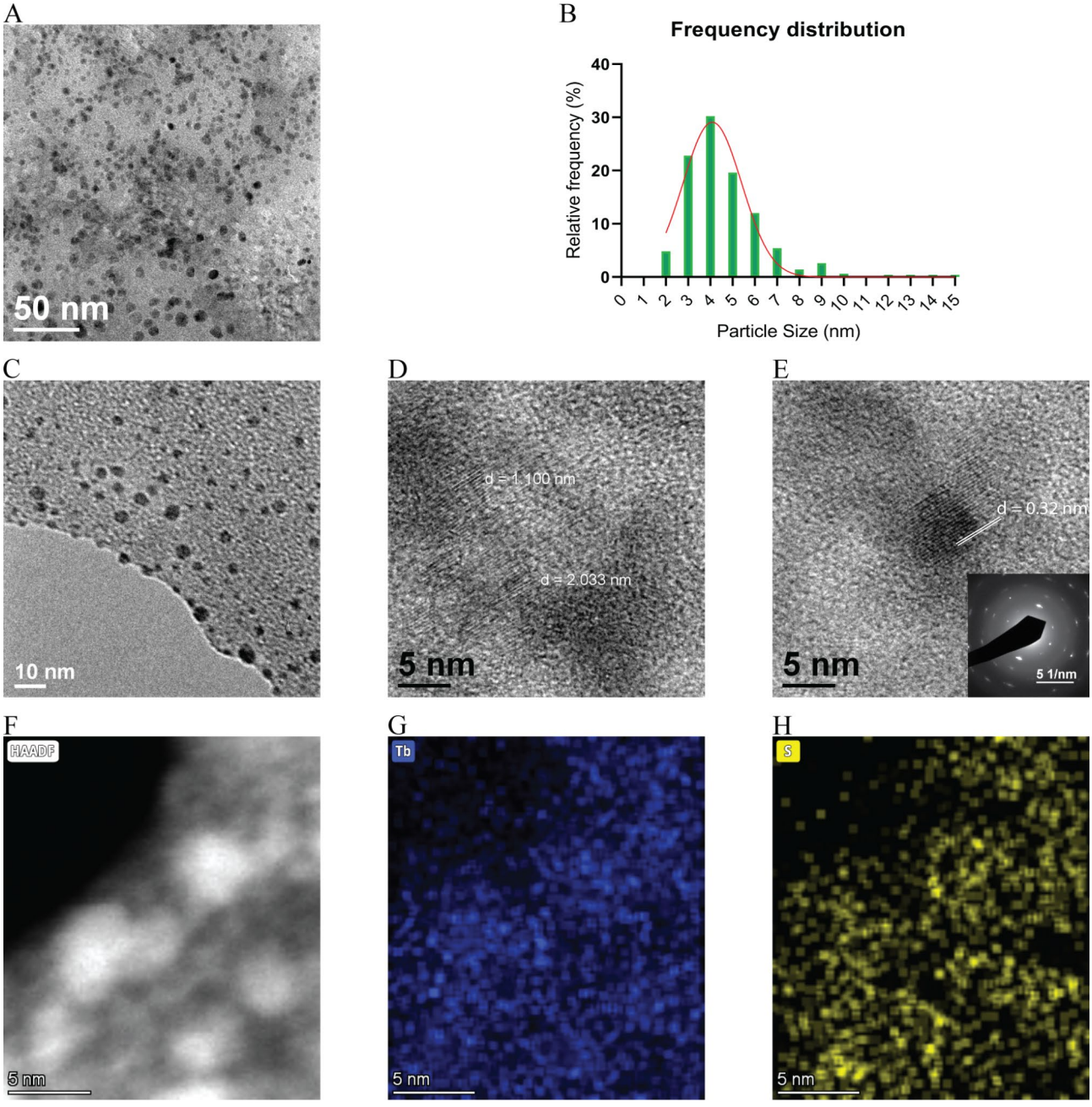

Fig. 2 Transmission electron microscopy characterization of purified TbS NPs produced by *E. coli*. (**A**) TEM micrograph of purified TbS NPs. (**B**) Size frequency distribution of purified NPs. (**C, D, E**) High resolution TEM micrographs of the biosynthesized TbS NPs. The inset in Figure E shows the selected area electron diffraction pattern obtained in the TEM. (**E**) STEM-HAADF image and the corresponding EDS elemental maps showing (**G**) sulfur and (**H**) terbium localization

The accumulation of REEs by different Gram-positive bacteria has been studied, but the effect on growth or viability has not been evaluated [47]. The MIC of terbium nitrate for *E. coli* has been previously reported to be above 1 mM which is consistent with the MIC values determined in our study on LB (3.5 mM) and R2A (0.5 mM) media (Figure S1) [24]. Our results further revealed that the presence of Tb resulted in a 100% decrease in viability in *E. coli* cells exposed for 30 min to 10 or 3 mM terbium nitrate in LB and R2A media, respectively (Figure S2A and Figure S2B, respectively).

In general, cellular growth and viability of *E. coli* cells are less affected by Tb^{3+} in LB media than in R2A media, probably due to the higher concentration of biomolecules like proteins and vitamins present in LB media that can arrest heavy metals [48–50]. Another explanation could

be related to differential solubility of the REE in the two media [51–53]. In general, Tb toxicity on microbial cells has been attributed in part to the oxidation of unsaturated fatty acids in membrane lipids, changes in membrane proteins, and a decrease in membrane fluidity [21]. Exposure to Tb may induce DNA damage and abnormalities in the ammonia metabolism of cnidarians [54]. Additionally, protein-protein network analysis has shown that lanthanides may disrupt biosynthetic pathways involved in calcium-regulated processes by enzyme inhibition in *Saccharomyces cerevisiae* [55]. However, the toxic effects of REEs on bacteria have been scarcely studied to date. Thus, our results add to the limited knowledge regarding the interaction of Tb with bacterial cells.

Our results indicated a significant decrease in toxicity of terbium in cells treated with cysteine (Figure S3). Also, sulfide concentration in the headspace of cultures decreases in cells exposed to Tb (Figure S4). Additionally, the autometallography assay results detected the formation of metal sulfide structures on the purified NPs produced by *E. coli* in the presence of $Tb(NO_3)_3$ (Figure S6). This assay has been previously reported as a good detection method for metal-sulfide NPs [29–31]. Moreover, high-resolution transmission electron microscopy (HR-TEM) confirmed the formation of nanoparticles. These observations imply that sulfide interacts with Tb^{3+} to form TbS nanoparticles.

Metallic NPs biosynthesis has been reported to reduce the toxicity of metals in cells [56–58]. Maleke and colleagues reported the biomineralization and bioaccumulation of europium by a thermophilic metal-resistant bacterium [59]. Fischer and colleagues showed that *Anabaena spec*., a multicellular cyanobacterium, accumulates and incorporates Europium particles [60]. Considering all this, we propose that the overproduction of hydrogen sulfide by the modulation of the bacterial sulfur metabolism leads to the formation of extracellular TbS nanoparticles that spatially confine the terbium ions in NPs. Thus, Tb ions are no longer available to interact with the cell, and NP formation serves as a bacterial lanthanide detoxification mechanism.

Note that this biosynthesis method would involve the bacterial enzyme L-cysteine desulfhydrase to produce high amounts of hydrogen sulfide which then reacts with terbium nitrate to form TbS NPs. Other groups, including ours, have exploited the activity of this enzyme to produce metal-sulfide nanoparticles [35, 61, 62]. Additionally, the metal sequestration and tolerance mechanisms involving cysteine and cysteine-rich biomolecules that enhance the biosynthesis of NPs have been reported [63, 64].

The NPs produced by *E. coli* were purified and characterized. A fluorescence emission spectrum corresponding to Tb-based NPs, with narrow peaks at 488 nm, 545 nm, 585 nm, and 620 nm after excitation at 350 nm, was determined (Fig. 1B) [38–40]. These emission peaks correspond to the energetic transitions: $^5D_4 \rightarrow {}^7F_6$ (490 nm emission); $^5D_4 \rightarrow {}^7F_5$ (546 nm emission); $^5D_4 \rightarrow {}^7F_4$ (586 nm emission) and $^5D_4 \rightarrow {}^7F_3$ (622 nm emission). The total QY calculated was 28.3%, which is relatively high for pure REE NPs. Additionally, considering the rapid development and importance of time-gated fluorescence applications, we evaluated the fluorescence lifetime of the NPs. We report here a fluorescence lifetime of ~2 ms (Fig. 1C). It's important to note that the tuning of this property is fundamental for last-generation fluorescence applications, especially in bioimaging where the autofluorescence of the samples reduces immensely the resolution of the technique and time-gating imaging resolves this problem. Also, different lifetimes can be measured as distinct signals, thus enabling the possibility of generating multiple biolabels. Also, a slight increase in emission lifetime was observed for the NPs produced at lower Tb nitrate concentrations (Supplementary Figure S8). The change in emission lifetime might be related to changes in ligands bound to the NP, which could be explained by a difference in the biomolecules in the organic matrix where the NPs are embedded [38]. This emission lifetime is long enough to perform time-gated imaging and similar techniques [65, 66].

To the best of our knowledge, our method produces the smallest TbS NPs reported to date (Fig. 2B). Also, ultrasmall NPs below 6 nm have been reported to efficiently pass through the pores of the glomerulus in the kidneys, being rapidly eliminated from the circulatory system *via* the bladder and urine, which is desirable in biomedical applications to avoid any long-term side effects. Ultrasmall NPs also have specific pharmacokinetic properties and good tissue penetration. Moreover, surface modifications would greatly change their properties, in contrast with larger NPs that are less affected by their surface characteristics [67].

The electron diffraction patterns obtained through SAED match multiple known terbium sulfide crystal phases but are not consistent with terbium oxides or oxysulfides (Inset in Fig. 2E, Figure S10, Figure S11, Table S1, Table S2 and Table S3) [33]. Thus, we conclude that the nanoparticles comprise one or more crystalline terbium sulfide phases, but the multiple 2-θ angle peaks that are common for multiple terbium sulfides preclude us from confidently identifying which exact crystalline phase(s) are present. To date, XRD analysis and Raman analysis has also been inconclusive as the highest peaks are masked by the background signal from biomolecules (data not shown). Also, it is worth mentioning that it's possible that some of the product is amorphous, which complicates the crystal characterization.

EDS analysis confirmed the co-location of Tb and S, with a Tb to S ratio of 1.91 (Fig. 2G and H and Table S4). We thoroughly washed the nanoparticles to remove any remaining free cysteine from the media and further purified them using a thiol-sepharose column. However, it's possible that some cysteine may still be bound to the biomass.

Furthermore, the high mass percentages of C, N, O, and Na detected, along with dynamic light scattering (DLS) measurements showing a hydrodynamic size of approximately 10 nm—which is larger than the size observed via TEM—strongly suggest that the nanoparticles are embedded in an organic matrix, as has been previously reported for the biosynthesis of metal sulfide nanoparticles by microorganisms [68]. In conclusion, our results confirmed that *E. coli* is biosynthesizing crystalline TbS NPs.

To evaluate the cytotoxicity of the NPs, live/dead cell and MTT assays were performed (Figure S12). Increasing concentrations of Tb nitrate further reduced cell viability, resulting in almost no viable cells at concentrations ≥ 10 mg/mL. In contrast, exposure to TbS NPs revealed lower cytotoxicity than Tb nitrate (Supplementary Figure S12). In live/dead cell assays, no dead cells were visible after exposure to TbS NPs, whereas exposure to 10 mg/mL of terbium nitrate resulted in only dead cells being observed (Figure S14). These data suggest that Tb nitrate and TbS NPs affect cell viability via different mechanisms. That is, one might infer that the TbS NPs inactivated the metabolism of the cells, without disrupting the membrane, such that the dye cannot enter the cells, which therefore show no red fluorescence [69, 70]. Other reports showed similar results, where the lanthanide NPs are remarkably less toxic than the corresponding soluble Ln salts [71, 72]. Further investigation is required to determine how the NPs and the Ln salts affect viability and cell growth. Additionally, some discrepancies have been observed in these types of assays, where the NPs negatively affect the proliferation rate of one cell line and affect positively another cell line [73].

The development of the first biological method to produce TbS NPs and the characterization of the nanostructures produced provides a solid foundation to improve their properties in future research and to generalize the synthesis to other rare-earth sulfides. The NPs could also be functionalized with chelating ligands that photosensitize the NPs. This phenomenon is known as the antenna effect, where the ligand transfers its energy to the nanoparticle, resulting in increased emission from the lanthanide (38). This approach could involve functionalizing the nanoparticles with a bithiol ligand such as 1,2-Ethanedithiol (EDT) or a disulfide ligand like dithiobis(succinimidyl propionate) (DSP), conjugated to a light-absorbing molecule. This ligand would exhibit a strong affinity for the thiol groups present on the TbS nanoparticles, which were also utilized in the purification process using thiol-Sepharose 4B columns. Subsequently, another functional group would remain available for the attachment of a photosensitizer.

Conclusions

This study represents a significant advance in the nascent field of REE-based NP biosynthesis. The chemical synthesis of specific REE-based nanoparticles has been studied extensively, e.g., in the case of REE-doped fluoride phases. However, few reports on the synthesis of REE sulfides are available. Most methods employed to synthesize lanthanide sulfide and oxysulfide NPs use temperatures above 100 °C for extended times and there is no general method to control the size of the lanthanide sulfide NPs [76,77]. From this perspective, the novel method to biosynthesize ultrasmall terbium sulfide NPs we report here could have substantial impact. Moreover, several biosynthesis parameters, including precursor concentration, solution pH, temperature, and time of synthesis, remain available to tune the size, shape, and optical properties of the NPs. In summary, the results presented demonstrate that the biosynthesis method reported in this work allows *E. coli* to produce TbS NPs with spherical shape, average size below 5 nm, a size that has not been achieved by chemical methods, and interesting spectroscopic properties including a high emission quantum yield of 28.3% and an emission lifetime of ~ 2 ms, associated with the presence of Tb in the core of the NPs.

Abbreviations

DSP	Dithiobis (succinimidyl propionate)
DLS	Dynamic Light Scattering
DO_{600}	Optical Density measured at 600 nm
E. coli	Escherichia coli
EDP	Electron Diffraction Pattern
EDS	Energy Dispersive X-ray Spectroscopy
EDT	1,2-Ethanedithiol
HR-TEM	High Resolution Transmission Electron Microscopy
LanM	Lanmodulin
LB	Luria Bertani media
Ln^{3+}	Trivalent lanthanides
MDH	Methanol Dehydrogenase
MeS	Metal Sulfide
MIC	Minimum Inhibitory Concentration
NPs	Nanoparticles
QDs	Quantum Dots
QY	Quantum Yield
R2A	Reasoner's 2 A media
REE	Rare Earth Elements
SAED	Selected Area Electron Diffraction
Tb	Terbium
TbS	Terbium Sulfide
TEM	Transmission Electron Microscopy
UV	Ultraviolet
XRD	X-ray diffraction

Supplementary Information

The online version contains supplementary material available at https://doi.org/10.1186/s12934-024-02519-6.

Supplementary Material 1

Acknowledgements

Dedication: "In the loving memory of Claudio Vásquez Guzmán, an excellent friend, mentor, and scientist, but an even better human being. Thanks for all the adventures and for showing us the beauty of science and friendship" (JP-D).

Author contributions

J.J.L.: conceptualization, investigation, formal analysis, methodology, project administration, visualization, writing—original draft, and writing—review and editing; N.O.: project administration, writing—original draft, and writing—review and editing; N.T.: conceptualization, investigation, formal analysis, methodology, visualization, writing—original draft, and writing—review and editing; N.B.: conceptualization, investigation, formal analysis, methodology, visualization, writing—original draft, and writing—review and editing; E.O.: conceptualization, investigation, formal analysis, methodology, and writing—review and editing; P.L.: conceptualization, investigation, formal analysis, methodology, visualization, writing—original draft, and writing—review and editing; A.K.: conceptualization, investigation, formal analysis, methodology, visualization, writing—original draft, and writing—review and editing; K.C.: investigation, formal analysis, methodology, and writing—review and editing; S.A.: conceptualization, formal analysis, methodology, project administration, visualization, writing—original draft, and writing—review and editing; B.P.: project administration, visualization and writing—review and editing; P.P.: conceptualization, funding acquisition, project administration, and writing—review and editing; M.S.: conceptualization, funding acquisition, project administration, and writing—review and editing; J.P.-D.: conceptualization, funding acquisition, project administration, and writing—review and editing. All authors have read and agreed to the published version of the manuscript.

Funding

This material is based on research sponsored by the Air Force Research Laboratory (AFRL) and Defense Advanced Research Projects Agency (DARPA) under agreement number FA8650-22-2-7218. The U.S. Government is authorized to reproduce and distribute reprints for Governmental purposes notwithstanding any copyright notation thereon. This work was also supported by Fondo Nacional de Desarrollo Científico y Tecnológico (Fondecyt) grant number 1200870 (JMP-D).

Data availability

No datasets were generated or analysed during the current study.

Declarations

Ethics approval and consent to participate

Not aplicable.

Consent for publication

Not aplicable.

Competing interests

The authors declare no competing interests.

Received: 23 April 2024 / Accepted: 2 September 2024
Published online: 12 September 2024

References

1. Bao G, Wen S, Lin G, Yuan J, Lin J, Wong K-L, Bünzli J-CG, Jin D. Learning from Lanthanide complexes: the Development of Dye-Lanthanide nanoparticles and their Biomedical Applications. Coord Chem Rev. 2021;429:213642. https://doi.org/10.1016/j.ccr.2020.213642.
2. Duchna M, Cieślik I. Rare Earth Elements in New Advanced Engineering Applications. In *Rare Earth Elements - Emerging Advances, Technology Utilization, and Resource Procurement*; T. Aide, M., Ed.; IntechOpen, 2023. https://doi.org/10.5772/intechopen.109248
3. Fan Q, Cui X, Guo H, Xu Y, Zhang G, Peng B. Application of Rare Earth-Doped nanoparticles in Biological Imaging and Tumor Treatment. J Biomater Appl. 2020;35(2):237–63. https://doi.org/10.1177/0885328220924540.
4. Blasse G. Chapter 34 Chemistry and Physics of R-Activated phosphors. Handbook on the Physics and Chemistry of Rare Earths. Volume 4. Elsevier; 1979. pp. 237–74. https://doi.org/10.1016/S0168-1273(79)04007-1.
5. Yuan J, Wang G. Lanthanide-based luminescence probes and time-resolved luminescence bioassays. TrAC Trends Anal Chem. 2006;25(5):490–500. https://doi.org/10.1016/j.trac.2005.11.013.
6. Kusrini E, Safira AI, Usman A, Prasetyanto EA, Nugrahaningtyas KD, Santosa SJ, Wilson LD. Nanocomposites of Terbium Sulfide nanoparticles with a Chitosan Capping Agent for Antibacterial Applications. J Compos Sci. 2023;7(1):39. https://doi.org/10.3390/jcs7010039.
7. Chen Y, Chi Y, Wen H, Lu Z. Sensitized luminescent Terbium nanoparticles: Preparation and Time-resolved fluorescence assay for DNA. Anal Chem. 2007;79(3):960–5. https://doi.org/10.1021/ac061477h.
8. Charpentier C, Cifliku V, Goetz J, Nonat A, Cheignon C, Cardoso Dos Santos M, Francés-Soriano L, Wong K, Charbonnière LJ, Hildebrandt N. Ultrabright Terbium nanoparticles for FRET biosensing and in situ imaging of epidermal growth factor Receptors**. Chem – Eur J. 2020;26(64):14602–11. https://doi.org/10.1002/chem.202002007.
9. Lai C-H, Lu M-Y, Chen L-J, Metal. Sulfide nanostructures: Synthesis, Properties and Applications in Energy Conversion and Storage. J Mater Chem. 2012;22(1):19–30. https://doi.org/10.1039/C1JM13879K.
10. Fei W, Zhang M, Fan X, Ye Y, Zhao M, Zheng C, Li Y, Zheng X. Engineering of Bioactive Metal Sulfide nanomaterials for Cancer Therapy. J Nanobiotechnol. 2021;19(1):93. https://doi.org/10.1186/s12951-021-00839-y.
11. Tiseanu C, Mehra RK, Kho R, Kumke M. Comparative study of time-resolved Photoluminescence properties of Terbium-Doped Thiosalicylic-Capped CdS and ZnS Nanocrystals. J Phys Chem B. 2003;107(44):12153–60. https://doi.org/10.1021/jp035322e.
12. Tiseanu C, Mehra RK, Kho R. Optical response of Thiosalicylic-Capped CdS nanocrystals to Terbium ions. J Photochem Photobiol Chem. 2005;173(2):169–73. https://doi.org/10.1016/j.jphotochem.2005.01.017.
13. Debnath GH, Chakraborty A, Ghatak A, Mandal M, Mukherjee P. Controlled Terbium(III) luminescence in Zinc Sulfide nanoparticles: an Assessment of competitive photophysical processes. J Phys Chem C. 2015;119(42):24132–41. https://doi.org/10.1021/acs.jpcc.5b07182.
14. Poornaprakash B, Chalapathi U, Suh Y, Vattikuti SVP, Reddy MSP, Park S-H. Terbium-Doped ZnS Quantum dots: Structural, Morphological, Optical, Photoluminescence, and Photocatalytic Properties. Ceram Int. 2018;44(10):11724–9. https://doi.org/10.1016/j.ceramint.2018.03.250.
15. Shkir M, Chandekar KV, Alshahrani T, Kumar A, AlFaify SA. Novel Terbium Doping Effect on Physical properties of lead Sulfide nanostructures: a facile synthesis and characterization. J Mater Res. 2020;35(20):2664–75. https://doi.org/10.1557/jmr.2020.216.
16. Fu J, Wang L, Chen H, Bo L, Zhou C, Chen JA. Selective fluorescence probe for Mercury Ion based on the fluorescence quenching of Terbium(III)-Doped Cadmium Sulfide Composite nanoparticles. Spectrochim Acta Mol Biomol Spectrosc. 2010;77(3):625–9. https://doi.org/10.1016/j.saa.2010.06.038.
17. Fitriyanto NA, Fushimi M, Matsunaga M, Pertiwiningrum A, Iwama T, Kawai K. Molecular structure and Gene Analysis of Ce3+-Induced methanol dehydrogenase of Bradyrhizobium Sp. MAFF211645. J Biosci Bioeng. 2011;111(6):613–7. https://doi.org/10.1016/j.jbiosc.2011.01.015.
18. Hibi Y, Asai K, Arafuka H, Hamajima M, Iwama T, Kawai K. Molecular structure of La3+-Induced methanol dehydrogenase-like protein in Methylobacterium Radiotolerans. J Biosci Bioeng. 2011;111(5):547–9. https://doi.org/10.1016/j.jbiosc.2010.12.017.
19. Nakagawa T, Mitsui R, Tani A, Sasa K, Tashiro S, Iwama T, Hayakawa T, Kawai K. A Catalytic role of XoxF1 as La3+-Dependent methanol dehydrogenase in Methylobacterium Extorquens strain AM1. PLoS ONE. 2012;7(11):e50480. https://doi.org/10.1371/journal.pone.0050480.
20. Cotruvo JA, Featherston ER, Mattocks JA, Ho JV, Laremore TN, Lanmodulin. A highly selective lanthanide-binding protein from a lanthanide-utilizing bacterium. J Am Chem Soc. 2018;140(44):15056–61. https://doi.org/10.1021/jacs.8b09842.
21. Yang Q, Wang L, Zhou Q, Huang X. Toxic effects of Heavy Metal Terbium Ion on the composition and functions of cell membrane in horseradish

roots. Ecotoxicol Environ Saf. 2015;111:48–58. https://doi.org/10.1016/j.ecoenv.2014.10.002.
22. Jiang N, Wang L, Lu T, Huang X. Toxic effect of Terbium Ion on horseradish cell. Biol Trace Elem Res. 2011;143(3):1722–8. https://doi.org/10.1007/s12011-011-8968-2.
23. Rim KT, Koo KH, Park JS. Toxicological evaluations of Rare Earths and their health impacts to workers: a Literature Review. Saf Health Work. 2013;4(1):12–26. https://doi.org/10.5491/SHAW.2013.4.1.12.
24. Martínez Meroño RM. The Effect of Lanthanides and their nanoparticles on pathogenic Bacteria. Universitat Politècnica de València; 2020.
25. Park DM, Reed DW, Yung MC, Eslamimanesh A, Lencka MM, Anderko A, Fujita Y, Riman RE, Navrotsky A, Jiao Y. Bioadsorption of Rare Earth Elements through Cell Surface Display of Lanthanide binding tags. Environ Sci Technol. 2016;50(5):2735–42. https://doi.org/10.1021/acs.est.5b06129.
26. Brewer A, Chang E, Park DM, Kou T, Li Y, Lammers LN, Jiao Y. Recovery of Rare Earth elements from geothermal fluids through bacterial cell surface adsorption. Environ Sci Technol. 2019;53(13):7714–23. https://doi.org/10.1021/acs.est.9b00301.
27. Iram S, Khan S, Ansary AA, Arshad M, Siddiqui S, Ahmad E, Khan RH, Khan MS. Biogenic Terbium Oxide nanoparticles as the Vanguard against Osteosarcoma. Spectrochim Acta Mol Biomol Spectrosc. 2016;168:123–31. https://doi.org/10.1016/j.saa.2016.05.053.
28. Gallardo C, Monrás JP, Plaza DO, Collao B, Saona LA, Durán-Toro V, Pérez-Donoso JM. Low-temperature biosynthesis of fluorescent semiconductor nanoparticles (CdS) by oxidative stress resistant Antarctic bacteria. J Biotechnol. 2014;187:108–15.
29. Bruna N, Galliani E, Oyarzún P, Bravo D, Fuentes F, Pérez-Donoso JM. Biomineralization of Lithium nanoparticles by Li-Resistant Pseudomonas Rodhesiae isolated from the Atacama Salt flat. Biol Res. 2022;55(1):12. https://doi.org/10.1186/s40659-022-00382-6.
30. Loumbourdis NS, Danscher G. Autometallographic Tracing of Hg–S Quantum Dots in Frogs Exposed to Inorganic Mercury. *BioMetals* 2008, *21* (3), 311–319. https://doi.org/10.1007/s10534-007-9120-9
31. Danscher G, Stoltenberg M, Bruhn M, Søndergaard C, Jensen D. Immersion autometallography: histochemical in situ capturing of Zinc ions in Catalytic Zinc-Sulfur nanocrystals. J Histochem Cytochem. 2004;52(12):1619–25. https://doi.org/10.1369/jhc.4A6371.2004.
32. Schindelin J, Arganda-Carreras I, Frise E, Kaynig V, Longair M, Pietzsch T, Preibisch S, Rueden C, Saalfeld S, Schmid B, Tinevez J-Y, White DJ, Hartenstein V, Eliceiri K, Tomancak P, Cardona A. Fiji: an Open-Source platform for Biological-Image analysis. Nat Methods. 2012;9(7):676–82. https://doi.org/10.1038/nmeth.2019.
33. Liu H, Foley M, Lin Q, Liu J. EDP2XRD: a computer program for converting electron diffraction patterns into X-ray diffraction patterns. J Appl Crystallogr. 2016;49(2):636–41.
34. Bajaj B, Lei P, Andreadis ST. High efficiencies of gene transfer with immobilized recombinant retrovirus: kinetics and optimization. Biotechnol Prog. 2001;17(4):587–96. https://doi.org/10.1021/bp010039n.
35. Órdenes-Aenishanslins N, Anziani-Ostuni G, Monrás JP, Tello A, Bravo D, Toro-Ascuy D, Soto-Rifo R, Prasad PN, Pérez-Donoso JM. Bacterial synthesis of Ternary CdSAg Quantum dots through Cation Exchange: tuning the Composition and properties of Biological nanoparticles for Bioimaging and Photovoltaic Applications. Microorganisms. 2020;8(5):631. https://doi.org/10.3390/microorganisms8050631.
36. Venegas FA, Saona LA, Monrás JP, Órdenes-Aenishanslins N, Giordana MF, Ulloa G, Collao B, Bravo D, Pérez-Donoso JM. Biological Phosphorylated molecules participate in the Biomimetic and Biological synthesis of Cadmium Sulphide Quantum dots by promoting H_2S release from Cellular Thiols. RSC Adv. 2017;7(64):40270–8. https://doi.org/10.1039/C7RA03578K.
37. Shatalin K, Shatalina E, Mironov A, Nudler E. H_2S: a Universal Defense against antibiotics in Bacteria. Science. 2011;334(6058):986–90. https://doi.org/10.1126/science.1209855.
38. Hernández-Adame L, Méndez-Blas A, Ruiz-García J, Vega-Acosta JR, Medellín-Rodríguez FJ, Palestino G, Synthesis. Characterization, and Photoluminescence properties of Gd:Tb Oxysulfide Colloidal particles. Chem Eng J. 2014;258:136–45. https://doi.org/10.1016/j.cej.2014.07.067.
39. Yan X, Fern GR, Withnall R, Silver J. Effects of the Host Lattice and Doping Concentration on the Colour of Tb3 + Cation Emission in Y2O2S:Tb3 + and Gd2O2S:Tb3 + nanometer sized Phosphor particles. Nanoscale. 2013;5(18):8640. https://doi.org/10.1039/c3nr01034a.
40. Goetz J, Nonat A, Diallo A, Sy M, Sera I, Lecointre A, Lefevre C, Chan CF, Wong K-L, Charbonnière LJ. Ultrabright Lanthan Nanopart ChemPlusChem. 2016;81(6):526–34. https://doi.org/10.1002/cplu.201600007.
41. Lin S-L, Liu T-Y, Lo C-L, Wang B-S, Lee Y-J, Lin K-Y, Chang CA. Synthesis, surface modification, and photophysical studies of Ln2O2S:Ln′3+ (ln = gd, tb, Eu; Ln′=Tb and/ or Eu) nanoparticles for luminescence bioimaging. J Lumin. 2016;175:165–75. https://doi.org/10.1016/j.jlumin.2016.01.037.
42. Bhardwaj R, Gupta A, Garg JK. Impact of Heavy metals on Inhibitory Concentration of Escherichia Coli—a case study of River Yamuna System, Delhi, India. Environ Monit Assess. 2018;190(11):674. https://doi.org/10.1007/s10661-018-7061-0.
43. Ghazisaeedi F, Ciesinski L, Bednorz C, Johanns V, Pieper L, Tedin K, Wieler LH, Günther S. Phenotypic zinc resistance does not correlate with Antimicrobial Multi-resistance in Fecal E. Coli isolates of piglets. Gut Pathog. 2020;12:4. https://doi.org/10.1186/s13099-019-0342-5.
44. Moreira Martins PM, Gong T, De Souza AA, Wood TK. Copper kills Escherichia Coli Persister Cells. Antibiotics. 2020;9(8):506. https://doi.org/10.3390/antibiotics9080506.
45. Qin W, Liu X, Yu X, Chu X, Tian J, Wu N. Identification of Cadmium Resistance and Adsorption Gene from Escherichia Coli BL21 (DE3). RSC Adv. 2017;7(81):51460–5. https://doi.org/10.1039/C7RA10656D.
46. Tsuruta T. Selective accumulation of light or heavy rare earth elements using gram-positive bacteria. Colloids Surf B. 2006;52(2):117–22. https://doi.org/10.1016/j.colsurfb.2006.04.014.
47. El Hajj S, Irankunda R, Camaño Echavarría JA, Arnoux P, Paris C, Stefan L, Gaucher C, Boschi-Muller S, Canabady-Rochelle L. Metal-chelating activity of soy and pea protein hydrolysates obtained after different enzymatic treatments from protein isolates. Food Chem. 2023;405:134788. https://doi.org/10.1016/j.foodchem.2022.134788.
48. Vandenbossche M, Jimenez M, Casetta M, Traisnel M. Remediation of Heavy metals by biomolecules: a review. Crit Rev Environ Sci Technol. 2015;45(15):1644–704. https://doi.org/10.1080/10643389.2014.966425.
49. Zhu K-X, Wang X-P, Guo X-N. Isolation and characterization of zinc-chelating peptides from wheat germ protein hydrolysates. J Funct Foods. 2015;12:23–32. https://doi.org/10.1016/j.jff.2014.10.030.
50. Di Bernardo P, Melchior A, Tolazzi M, Zanonato PL. Thermodynamics of Lanthanide(III) Complexation in Non-aqueous solvents. Coord Chem Rev. 2012;256(1–2):328–51. https://doi.org/10.1016/j.ccr.2011.07.010.
51. Judge WD, Ng KL, Moldoveanu GA, Kolliopoulos G, Papangelakis VG, Azimi G. Solubilities of Heavy Rare Earth Sulfates in Water (Gadolinium to Lutetium) and H2SO4 solutions (dysprosium). Hydrometallurgy. 2023;218:106054. https://doi.org/10.1016/j.hydromet.2023.106054.
52. Miyamoto H, Shimura H, Sasaki K. Solubilities of Rare Earth Iodates in Aqueous and Aqueous Alcoholic Solvent mixtures. J Solut Chem. 1985;14(7):485–97. https://doi.org/10.1007/BF00646980.
53. Blaise C, Gagné F, Harwood M, Quinn B, Hanana H. Ecotoxicity responses of the Freshwater Cnidarian Hydra Attenuata to 11 Rare Earth elements. Ecotoxicol Environ Saf. 2018;163:486–91. https://doi.org/10.1016/j.ecoenv.2018.07.033.
54. Pallares RM, Faulkner D, An DD, Hébert S, Loguinov A, Proctor M, Villalobos JA, Bjornstad KA, Rosen CJ, Vulpe C, Abergel RJ. Genome-Wide Toxicogenomic Study of the Lanthanides Sheds Light on the Selective Toxicity Mechanisms Associated with Critical Materials. *Proc. Natl. Acad. Sci.* 2021, *118* (18), e2025952118. https://doi.org/10.1073/pnas.2025952118
55. Kapoor RT, Salvadori MR, Rafatullah M, Siddiqui MR, Khan MA, Alshareef SA. Exploration of microbial factories for synthesis of Nanoparticles – A Sustainable Approach for Bioremediation of Environmental contaminants. Front Microbiol. 2021;12:658294. https://doi.org/10.3389/fmicb.2021.658294.
56. Mohseniazar M, Barin M, Zarredar H, Alizadeh S, Shanehbandi D. Potential of Microalgae and Lactobacilli in Biosynthesis of Silver nanoparticles. BioImpacts BI. 2011;1(3):149–52. https://doi.org/10.5681/bi.2011.020.
57. Ovais M, Khalil A, Ayaz M, Ahmad I, Nethi S, Mukherjee S. Biosynthesis of metal nanoparticles via Microbial enzymes: a mechanistic Approach. Int J Mol Sci. 2018;19(12):4100. https://doi.org/10.3390/ijms19124100.
58. Maleke M, Valverde A, Vermeulen J-G, Cason E, Gomez-Arias A, Moloantoa K, Coetsee-Hugo L, Swart H, Van Heerden E, Castillo J. Biomineralization and Bioaccumulation of Europium by a Thermophilic Metal Resistant Bacterium. Front Microbiol. 2019;10:81. https://doi.org/10.3389/fmicb.2019.00081.
59. Fischer CB, Körsten S, Rösken LM, Cappel F, Beresko C, Ankerhold G, Schönleber A, Geimer S, Ecker D, Wehner S. Cyanobacterial Promoted Enrichment of Rare Earth Elements Europium, Samarium and Neodymium and Intracellular

Europium particle formation. RSC Adv. 2019;9(56):32581–93. https://doi.org/10.1039/C9RA06570A.
60. Wei S, Guo C, Wang L, Xu J, Dong H. Bacterial synthesis of PbS nanocrystallites in one-step with l-Cysteine serving as both Sulfur source and capping Ligand. Sci Rep. 2021;11(1):1216. https://doi.org/10.1038/s41598-020-80450-7.
61. Xu H, Zhang P, He E, Peijnenburg WJGM, Cao X, Zhao L, Xu X, Qiu H. Natural formation of copper Sulfide nanoparticles via Microbially Mediated Organic Sulfur Mineralization in Soil: processes and mechanisms. Geoderma. 2023;430:116300. https://doi.org/10.1016/j.geoderma.2022.116300.
62. Bae W, Chen W, Mulchandani A, Mehra RK. Enhanced Bioaccumulation of Heavy metals by bacterial cells displaying synthetic phytochelatins. Biotechnol Bioeng. 2000;70(5):518–24. https://doi.org/10.1002/1097-0290(20001205)70:5%3C518::AID-BIT6%3E3.0.CO;2-5.
63. Park TJ, Lee SY, Heo NS, Seo TS. In vivo synthesis of Diverse Metal nanoparticles by recombinant Escherichia Coli. Angew Chem Int Ed. 2010;49(39):7019–24. https://doi.org/10.1002/anie.201001524.
64. Cardoso Dos Santos M, Goetz J, Bartenlian H, Wong K-L, Charbonnière LJ, Hildebrandt N. Autofluorescence-free live-cell imaging using Terbium nanoparticles. Bioconjug Chem. 2018;29(4):1327–34. https://doi.org/10.1021/acs.bioconjchem.8b00069.
65. Yao J, López-Peña G, Lifante J, Iglesias-de La Cruz MC, Marin R, Martín Rodríguez E, Jaque D, Ortgies DH. (INVITED)adjustable near-infrared fluorescence Lifetime Emission of Biocompatible Rare-Earth-Doped nanoparticles for in vivo Multiplexing. Opt Mater X. 2023;17:100225. https://doi.org/10.1016/j.omx.2022.100225.
66. Zarschler K, Rocks L, Licciardello N, Boselli L, Polo E, Garcia KP, De Cola L, Stephan H, Dawson KA. Ultrasmall Inorganic nanoparticles: State-of-the-art and perspectives for Biomedical Applications. Nanomed Nanotechnol Biol Med. 2016;12(6):1663–701. https://doi.org/10.1016/j.nano.2016.02.019.
67. Plastun IL, Zakharov AA, Naumov AA. Features of Silver Sulfide Nanoparticles Bacterial Synthesis: Molecular Modeling. In 2020 *International Conference on Actual Problems of Electron Devices Engineering (APEDE)*; IEEE: Saratov, Russia, 2020; pp 318–322. https://doi.org/10.1109/APEDE48864.2020.9255570
68. Choi JY, Lee SH, Na HB, An K, Hyeon T, Seo TS. In Vitro cytotoxicity screening of Water-Dispersible Metal Oxide nanoparticles in Human Cell lines. Bioprocess Biosyst Eng. 2010;33(1):21–30. https://doi.org/10.1007/s00449-009-0354-5.
69. Huang C-Y, Ger T-R, Wei Z-H, Lai M-F. Compare analysis for the Nanotoxicity effects of different amounts of endocytic Iron oxide nanoparticles at single cell level. PLoS ONE. 2014;9(5):e96550. https://doi.org/10.1371/journal.pone.0096550.
70. Joonas E, Aruoja V, Olli K, Syvertsen-Wiig G, Vija H, Kahru A. Potency of (Doped) Rare Earth Oxide particles and their Constituent metals to inhibit Algal Growth and induce direct toxic effects. Sci Total Environ. 2017;593–594:478–86. https://doi.org/10.1016/j.scitotenv.2017.03.184.
71. Kurvet I, Juganson K, Vija H, Sihtmäe M, Blinova I, Syvertsen-Wiig G, Kahru A. Toxicity of nine (Doped) Rare Earth Metal Oxides and Respective Individual metals to aquatic microorganisms Vibrio Fischeri and Tetrahymena Thermophila. Materials. 2017;10(7):754. https://doi.org/10.3390/ma10070754.
72. Heng BC, Das GK, Zhao X, Ma L-L, Tan TT-Y, Ng KW, Loo JS-C. Comparative cytotoxicity evaluation of Lanthanide nanomaterials on Mouse and Human Cell Lines with metabolic and DNA-Quantification assays. Biointerphases. 2010;5(3):FA88–97. https://doi.org/10.1116/1.3494617.
73. Fan, J. Z., La Croix, A. D., Yang, Z., Howard, E., Quintero-Bermudez, R., Levina, L., ... & Macdonald, J. E. (2019). Ligand cleavage enables formation of 1, 2-ethanedithiol capped colloidal quantum dot solids. Nanoscale, 11(22), 10774–10781.

Publisher's note